Action of strong internal solitary waves on surface waves

Victor V. Bakhanov
Institute of Applied Physics, Russian Academy of Sciences, Nizhny Novgorod, Russia

Lev A. Ostrovsky[1]
Zel Technologies/NOAA Environmental Technology Laboratory, Boulder, Colorado, USA

Received 29 June 2001; revised 26 October 2001; accepted 6 February 2002; published 2 October 2002.

[1] Transformation of gravity capillary surface waves on the current created by a large-amplitude internal wave (IW) is considered. The trajectories of surface wave packets in a domain of coordinate and wave number are calculated for different IW amplitudes. In particular, the location of maxima and minima of the surface wave (SW) spectral density W with respect to the IW profile is studied. It is shown that for sufficiently large-amplitude internal solitary waves (solitons) propagating in the same direction as the surface wave the minimum of W for all SW lengths is situated over the crest of the soliton. The corresponding "critical" value of the soliton amplitude is calculated. The noncollinear propagation of internal and surface waves is also considered. Finally, some numerical results obtained using the kinetic equation that describes the transformation of W in a field of large-amplitude internal wave solitons are presented that are in agreement with the qualitative description and with recent observations of radar scattering from strong internal waves in a coastal area. *INDEX TERMS:* 4572 Oceanography: Physical: Upper ocean processes; 4560 Oceanography: Physical: Surface waves and tides (1255); 0933 Exploration Geophysics: Remote sensing; 4544 Oceanography: Physical: Internal and inertial waves; *KEYWORDS:* internal waves, surface waves, wave interaction, remote sensing, soliton

Citation: Bakhanov, V. V., and L. A. Ostrovsky, Action of strong internal solitary waves on surface waves, *J. Geophys. Res.*, *107*(C10), 3139, doi:10.1029/2001JC001052, 2002.

1. Introduction

[2] The influence of internal gravity waves on wind waves has been discussed for several decades. The interest in this problem has increased especially since the development of remote sensing facilities that measure the effects of internal waves on the sea surface [*Hughes and Gower*, 1983; *Hughes and Dawson*, 1988; *Gasparovic et al.*, 1988; *Thompson et al.*, 1988; *Lyzenga and Bennett*, 1988; *Hogan et al.*, 1996; *Kropfli et al.*, 1999]. Usually the transformation of a wind-wave spectrum under the action of a nonuniform current created by internal waves is calculated numerically from the kinetic equation for the spectral density of wave energy or action. This is often associated with a rather cumbersome and physically unclear body of calculation. However, some important qualitative conclusions about the character of wind-wave spectrum transformation can be made from a much simpler analysis of surface wave kinematic characteristics such as wave packet trajectories and the wave vector variations in the internal wave field.

[3] For an internal wave soliton this approach was applied, apparently for the first time, by *West et al.* [1975] and *Thompson and West* [1975]. They have shown that surface wave groups can be reflected from the area of the internal wave soliton with an upward pycnocline displacement (both in forward and backward directions), which may significantly affect the SW spectrum. An example of calculation of the wave number variation for wave packets propagating parallel to a group of internal wave solitons was given by *Caponi et al.* [1988]. The results were presented in a coordinate-wave vector domain which revealed the existence of wave groups trapped by an internal wave. The group trajectories for surface gravity waves moving at an angle to the propagation direction of an IW soliton with negative pycnocline displacement were considered by *Gotwols et al.* [1988]. A detailed analysis of surface wave kinematics (variability of wave number) in a field of internal waves was carried out by *Basovich* [1979] for one-dimensional wave propagation through an internal soliton and by *Basovich and Bakhanov* [1984] for a two-dimensional problem when surface wave packets propagate under an arbitrary angle to a sinusoidal IW. Still, their consideration was confined by weak (linear) internal waves. In this case, significant variations of wave parameters occur for SWs whose group velocities projected on the propagation direction of the internal wave are close to the internal wave phase speed (group synchronism). These waves may be reflected and trapped even by a small internal wave current

[1]On leave from Institute of Applied Physics, Russian Academy of Sciences, Nizhny Novgorod, Russia.

0148-0227/02/2001JC001052$09.00

("blocking effect") [see *Phillips*, 1977; *Basovich and Talanov*, 1977]. For typical values of the IW speed, this effect is strongest for decimeter range SWs. Therefore, the trajectories of surface wave packets were constructed only for gravity surface waves rather than for capillary and gravity capillary waves.

[4] Our consideration here is based on the fact that in many cases the tide-generated IWs appear in the form of "solibores," i.e., trains of localized, solitary isopycnal depressions which we call here internal solitons (notwithstanding the more specific mathematical definition of a soliton). Moreover, in many cases these solitons are very strong in the sense that the displacement of isopycnal surfaces may be comparable with or even significantly larger than the initial depth of the pycnocline. A recent strong example of such behavior is the Coastal Ocean Probing Experiment (COPE) described by *Stanton and Ostrovsky* [1998] and *Kropfli et al.* [1999], where the IW solitons having amplitudes up to 25–27 m propagated on the background of a 5–7 m deep pycnocline. The current velocity in these solitons could be close to the wave phase velocity, which testifies to an extremely strong nonlinearity (up to an almost maximal amplitude at which a soliton would break). As a result, at different points of the solitary IW profile, the aforementioned blocking effect can occur for a broad range of wavelengths. In this situation the location of maxima and minima of surface wave spectral density registered in COPE was different from those predicted before. Note that these positions can be an important indicator for interpretation of radar scattering data.

[5] In this paper, a detailed analysis of the wave packet trajectories for gravity-capillary waves propagating over internal solitary waves of different amplitudes, including very strong ones, is presented. Based on kinematic approach, the distribution of the SW intensity over the soliton is evaluated, including the positions of maxima and minima of wave energy with respect to the current profile in the IW. We also give some calculations of the variability of surface wave spectral density by solving the kinetic equation, which confirms the qualitative analysis and agrees with the data of COPE as a typical example of very strong solitons in coastal zones.

2. Basic Equations

2.1. Equations for Space-Time Rays

[6] Propagation of a surface wave on a large-scale current $\mathbf{U} = \mathbf{U}(\mathbf{r}, t)$, where $\mathbf{r} = (x, y)$, is described by the known equations of space-time rays ("geometrical approximation") [e.g., *Basovich and Bakhanov*, 1984]:

$$\dot{\mathbf{r}} = \frac{\partial\omega(\mathbf{r},\mathbf{k},t)}{\partial\mathbf{k}}, \qquad \dot{\mathbf{k}} = -\frac{\partial\omega(\mathbf{r},\mathbf{k},t)}{\partial\mathbf{r}}, \tag{1}$$

where $\mathbf{k}$ and ω are wave vector and frequency of the wave packet (group) in the reference frame immovable with respect to bottom. The current created near the water surface by the internal wave

$$\mathbf{U} = U(x - Ct)\mathbf{x}_0 \tag{2}$$

is assumed to be known (the effect of SW on the current can be neglected [*Basovich*, 1982]). Here $\mathbf{x}_0$ is the unit vector in x direction. In the coordinate frame moving with phase speed of the internal wave (below it is called system C), the current determined by equation (2) is stationary and hence the wave packet frequency $\Omega = \omega - (\mathbf{x}_0, \mathbf{k})C$ remains constant. The motion of surface wave packets in system C is described by equation (1), where ω is replaced by Ω, which, in turn, is determined by the known dispersion equation

$$\Omega = -k_xC + k_xC\beta(\xi) + \sqrt{g\left(k_x^2 + k_y^2\right)^{1/2} + \nu\left(k_x^2 + k_y^2\right)^{3/2}}. \tag{3}$$

Here k_x and k_y are components of the horizontal wave vector (they are chosen parallel and perpendicular to the propagation direction of the internal wave, respectively), $\beta(\xi) = U/C$, $\xi = x - Ct$, and ν is the surface tension coefficient divided by the water density. The dispersion relation (3) is essentially the first integral of the system (1). It allows the construction of trajectories of the wave packets in variables ξ and $\mathbf{k}$. The y component is conserved along any fixed trajectory of the wave packet (group) provided the current created by the internal wave does not depend on y. Therefore, to describe the wave group propagation, it is necessary to consider only the projections of trajectories on the plane (ξ, k_x).

2.2. On Strongly Nonlinear Solitons

[7] Among the problems arising here is adequate description of current velocity in a strong IW for use in our calculations. Small and moderate-amplitude solitons are commonly described by the known Korteweg-de Vries (KdV) equation [e.g., *Ostrovsky and Stepanyants*, 1989]. However, as already noted, in a number of coastal zone observations such solitons are strongly nonlinear, and the classical KdV model is inapplicable; in particular, the width of observed solitons proves to be much larger than that predicted by KdV for the same amplitudes, their velocity is smaller, and the width is only weakly dependent on the amplitude in a wide range of parameters.

[8] No strict theory exists that describes strong IWs in a way analogous to the evolution KdV equation. For a two-layer model, computational results [e.g., *Amick and Turner*, 1986] show that a limiting soliton amplitude exists at which the wave tends to a pair of infinitely separated fronts (kinks). Similar properties follow from a simplified system obtained by *Choi and Camassa* [1999] which somewhat generalizes Boussinesq equations to stronger nonlinearity. However, observed solitons, even strongly nonlinear ones, do not approach this value of amplitude. Based on that, several simplified analytical models that reduce the problem to a one-dimensional evolution equation were later suggested [e.g., *Ostrovsky*, 1999]. However, only limited applicability or no analytical solutions exist for strong solitons even in these simplified equations. Thus, to avoid cumbersome expressions, we approximate pycnocline displacement (a depression in most shallow-water situations, i.e., $\eta < 0$) by a shape corresponding to a KdV soliton:

$$\eta = -\frac{\eta_0}{\cosh^2\left(\frac{x - Ct}{\Delta}\right)}, \tag{4}$$

where η_0 is maximal displacement (the soliton amplitude), and Δ is the characteristic width of the soliton. We, however, do not use the relationships between the parameters C, Δ, and η_0 following from the KdV equation because they are not valid for the observed strong solitons. Thus, equation (4) should be considered as a phenomenological approximation which coincide with the KdV solitons in the limit of weak nonlinearity.

[9] To calculate surface current from equation (4), a two-layer model will be used which can be considered as adequate for coastal zones with a sharp pycnocline (as in the case of COPE). The current velocity in the upper layer for a long stationary wave can readily be determined from the mass conservation condition as

$$\frac{U}{C} = \frac{-\eta}{h_1 - \eta}, \qquad (5)$$

where h_1 is the thickness of the upper layer (h_2 for the lower layer).

[10] In cases when the dependence between soliton velocity and its amplitude is necessary, we shall use a recent semiempirical model suggested by *Ostrovsky* [1999] which gives good agreement with observations if $h_1 \ll h_2$ that is the case in a number of coastal zone experiments. It is based on the exact description of very long progressive waves for which dispersion can be neglected, with an addition of a phenomenological nonlinear dispersive term. From that equation, the normalized soliton velocity can be well approximated by a polynomial

$$C/C_0 = 1 + 0.5s - 0.116s^2 + 0.0225s^3 - 0.0017s^4. \qquad (6)$$

Here $s = \eta_0/h_1$, $C_0 = \sqrt{g'h_1}$, $g' = g\Delta\rho/\rho$, g is the gravity acceleration, ρ is the density, and $\Delta\rho$ is the density difference of the layers (in the ocean $g' \ll g$). Note that the validity of this model under the conditions considered has been confirmed both by comparison with the *Choi and Camassa* [1999] model. It is easy to see that C_0 is the linear longwave velocity in the case considered (thin upper layer), and in this case, the ratio (6) does not depend on specific parameters of the layers. When dimensional values are needed for calculations, we used COPE data as an example on which to base our calculations, and accepted the following experimental values of parameters: $h_1 = 5$ m, $h_2 = 143$ m (hence the condition $h_1 \ll h_2$ is met), and the relative density change in the pycnocline $\Delta\rho/\rho = 0.002$. This particular hydrology will be considered for illustration, considering that the main effects associated with strongly nonlinear internal waves are of general applicability. Note that the approximation (6) differs from the numerical result by less than 1% for all $s < 5.5$, i.e., up to the soliton amplitudes of 27.5m (the full range of COPE data). In what follows, calculations were performed for different values of maximal pycnocline depressions.

3. Kinematics of Wave Packets

3.1. Collinear Propagation

[11] Consider now the surface wave group trajectories under the action of the current (equation (5)) in internal solitons of different amplitudes. These results will be used in the next section to describe transformation of surface wave spectral density, *W*. We begin with the one-dimensional case of collinear propagation of surface and internal waves ($k_y = 0$).

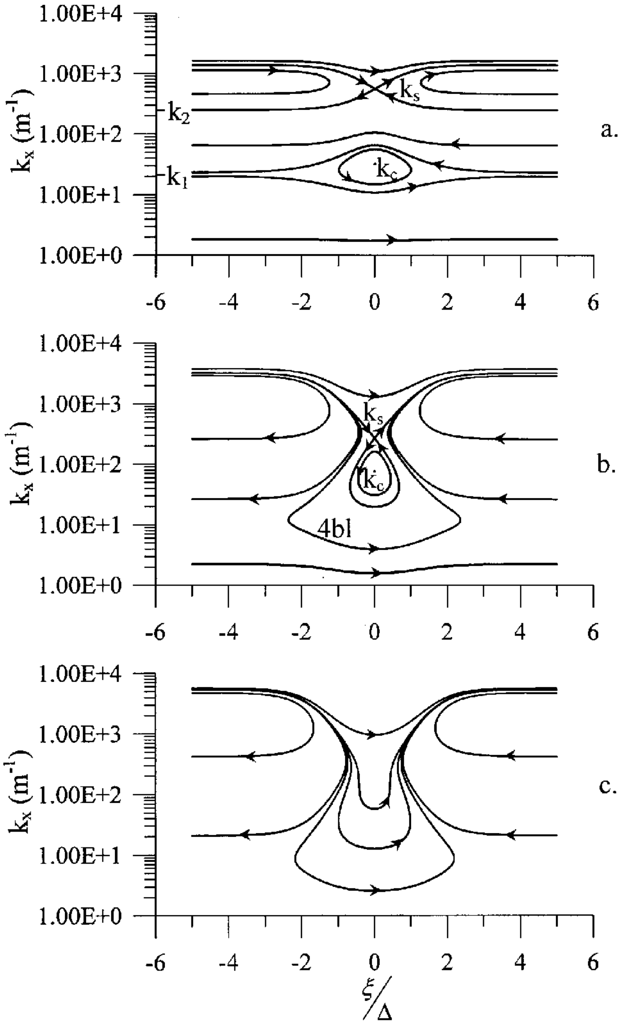

Figure 1. Trajectories of surface wave packets in a one-dimensional case ($k_y = 0$): (a) $\eta_0 = 1$ m, (b) $\eta_0 = 7$ m, and (c) $\eta_0 = 15$ m.

[12] The trajectories of surface wave packets (groups) on the (k_x, ξ) plane are shown in Figures 1a–1c for three values of soliton amplitude (wave numbers are plotted in logarithmic scale). The trajectories were calculated numerically from equations (3) to (6) for different values of Ω fixed at each trajectory.

[13] The figures readily show how the wavelength changes in the course of propagation of a given group. Figure 1a corresponds to a relatively small pycnocline displacement, $\eta_0 = 1$ m or, according to equation (5), $U_{max}/C = 0.17$. Here two stationary points exist where a packet can stay infinitely long over the soliton peak: a saddle, where $k = k_s$, that corresponds to surface wavelength $\lambda = 1.1$ cm, and a center at $k = k_c$, where $\lambda = 20$ cm. The closed trajectories around the center correspond to trapped wave groups localized in the vicinity of the soliton, whereas the others begin at infinity and pass through the soliton. For trajectories starting in the interval between the values k_1 and k_2 (see Figure 1a), the wave number grows upon propagation toward the soliton peak, and for the rest of the trajectories, it decreases.

[14] Trajectories also exist that do not reach the soliton peak at all but are reflected from some points at IW slopes. In these points, the well-known blocking effect occurs. Note that for these trajectories, the wave number grows at the leading edge of the soliton and decreases at its trailing edge.

[15] With the increase of η_0, the center is displaced upwards and the saddle downwards, and the variations of the surface wave number become stronger. Moreover, for some value of soliton amplitude, the picture changes qualitatively as a result of a bifurcation. In Figure 1b, the case of η_0 = 7 m or U_{max}/C = 0.58 is shown. There still exist two equilibrium points, a center and a saddle, but the separatrix (a trajectory going in/out of the saddle point) encloses the center so that all packets moving between center and saddle are now trapped by the internal wave. For the scales selected, the saddle corresponds to wavelength λ = 2.3 cm, and center, λ = 8.5 cm. The packets moving above the separatrix (large k) are passing through the soliton to infinity. The same is true for very small k (trajectories going well below the center). Other packets moving outside the separatrix are reflected after reaching a turning (blocking) point. It is interesting to note that there also exist trajectories (like the one marked as 4bl in Figure 1b) that do not reach minus infinity after the reflection but return to the right under the center, then go left, and are reflected again. These back-and-forth motions can repeat themselves more than once. Hence, the effects of "double blocking" and "quartic blocking" are possible.

[16] A further increase of η_0 leads to a new bifurcation: the saddle and the center coalesce and both disappear so that there are no trapped packets at all. Such a situation is shown in Figure 1c where η_0 = 15 m and U_{max}/C = 0.75. Note that in this case all wave packets reaching the soliton center decrease their wave number and all of them propagate locally faster that the soliton (at ξ = 0 all trajectories go from left to right).

3.2. Propagation in Different Directions

[17] In a similar way, surface wave propagation under a finite angle θ to the direction of internal wave propagation can be described. In general, plotting the wave packet trajectories in the three-dimensional coordinate-wave vector space would be most representative here. However, such a three-dimensional pattern is rather complicated. A common method is to plot again the dependencies $k_x(\xi)$ for a fixed value of k_y [*Basovich and Bakhanov*, 1984; *Gotwols et al.*, 1988]. However, under these conditions the wave propagation direction (defined by the ratio k_x/k_y) would vary strongly from one trajectory to another. Namely, longer waves (the bottom part of the corresponding figure) would propagate under large angles θ, whereas the top part of the figure (short waves) corresponds to small values of θ. This method does not seem to give a clear qualitative description of the behavior of wave groups. Here we chose a different ensemble of wave groups; namely, those propagating in the same direction (i.e., having the same ratio k_x/k_y) at the moment when they reach the soliton peak, i.e., the point ξ = 0. Evidently, these packets have different initial and final propagation directions, and the value of k_y, still remaining constant along each trajectory, differs for different trajectories. In this way we are able to describe the SWs having close propagation directions but a broad range of wavelengths when they approach the soliton peak.

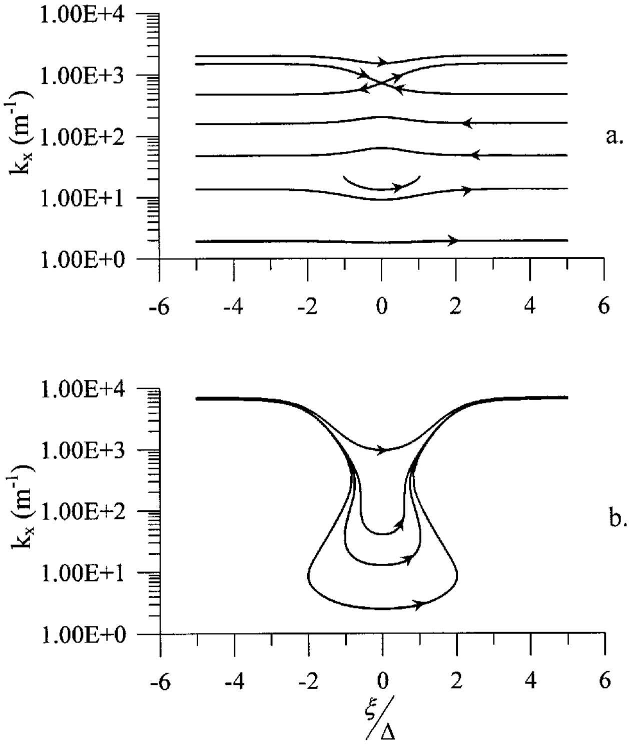

Figure 2. Trajectories of surface wave packets with θ = 30°: (a) η_0 = 1 m and (b) η_0 = 20 m.

[18] The corresponding trajectories of wave packets are shown in Figures 2a and 2b for θ = 30° over the soliton peak. For a weak internal wave when η_0 = 1 m (Figure 2a), they differ only slightly from the case θ = 0: the saddle moves a little upwards and the center a little downwards (the point k_s corresponds to λ = 0.9 cm and the point k_c corresponds to λ = 27 cm). Note that only a lower part of the trajectory is shown for the trapped groups (moving around the center). With the increase of soliton amplitude up to η_0 = 20 m and U_{max}/C = 0.8 (Figure 2b), the trajectories qualitatively correspond to Figure 1c in the one-dimensional case. In particular, for large solitons, at the point ξ = 0 all trajectories have the same sign of curvature, i.e., the second derivative $\partial^2 k_x/\partial\xi^2$ is positive at ξ = 0 for all trajectories (the effect of this parameter is explained below, before the formula (8)). However, for the bifurcation leading to the pattern shown in Figure 2b, larger soliton amplitudes are needed. That is why Figures 1c and 2b are shown for different η_0 (15 and 20 m, respectively).

[19] Upon increasing θ to 45°, groups still exist with a negative value of $\partial^2 k_x/\partial\xi^2$ in the point ξ = 0 even for internal wave amplitudes as large as 20 m (Figure 3). The bifurcation similar to that yielding the picture shown in Figure 2b occurs for even larger amplitudes. Note that the crossing of trajectory projections in Figure 3 does not, of course, mean crossing of real trajectories in the three-dimensional coordinate-wave vector space (except for, possibly, the equilibrium points), because the crossed curves correspond to various values of k_y. Note also that the variations of

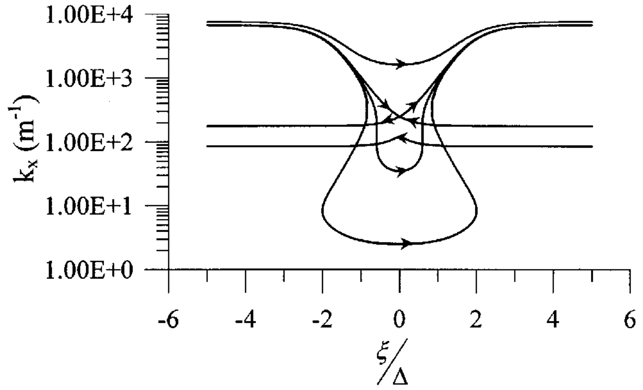

Figure 3. Trajectories of surface wave packets with $\theta = 45°$, $\eta_0 = 20$ m.

wave number for an SW propagating under a finite angle to the direction of internal wave propagation are typically smaller than those in the case $\theta = 0$.

4. Surface Wave Spectrum Transformation (Qualitative Analysis)

4.1. Relationship Between Variations of Wave Number and Wave Energy

[20] By using the analysis of wave packet trajectories performed above, one can consider how the spatial distribution of wave energy density, $W(\xi, \mathbf{k})$ will evolve due to IWs with different amplitudes η_0. In general, a kinetic equation with a given initial energy spectrum $W_0(\mathbf{k})$ incident on the IW region, must be solved as it shall be done here later. However, for better understanding, we start again from a simplified approach based on the results of the previous sections. As is known [e.g., *LeBlond and Mysak*, 1978], in the absence of wind forcing and dissipation, spectral density of surface wave action, N, remains constant at any fixed wave group trajectory. Therefore, the value of N at a given point $(\mathbf{r}, \mathbf{k})$ is equal to that at the initial point of the same trajectory where the internal wave current is absent. Here we use a common definition for the energy as a spectral integral of the correlation function of surface displacements, and for wave action as $N(\mathbf{r}, \mathbf{k}, t) = W(\mathbf{r}, \mathbf{k}, t)/\omega$, and all these quantities are taken in the reference frame of water, i.e. that moving with the local IW current velocity with respect to the bottom. This, in turn, defines the wave energy of a group, which in the same reference frame has the form:

$$W = N\sqrt{gk + \nu k^3} = N[\Omega + (C - U)k_x]. \quad (7)$$

[21] As a result, the energies of wave groups (proportional to mean square of displacements) and their wave vectors far from a soliton, W_0 and $\mathbf{k}_0$, completely determine the spatial distribution of wave action and energy in the perturbed area. This enables a qualitative description of wave energy modulation based on the evolution of the wave number in the groups plotted in Figures 1–3.

[22] In general, there are two sources of change of wave energy by the IW current. First, it changes adiabatically, according to equation (7) with $N = const$ for each trajectory. Second, initial spectral variations of $N_0(\mathbf{k})$ and $W_0(\mathbf{k})$ are carried along trajectories and bring different values of W from those existing over the soliton at the initial moment. These two factors form a rather complex pattern of space-time distribution of wave energy.

[23] To simplify the problem and adjust it to the remote sensing needs, we shall consider spatial distributions of W at a fixed wave number $\mathbf{k}_f$ and, in particular, the change of W (contrast) over the soliton maximum with respect to its value in the absence of IW. Indeed, only waves with a fixed $\mathbf{k}$ (or close to it) are often responsible for the radar scattering at a fixed wavelength (as in the case of Bragg scattering), so that variation of the energy of such waves shall define, at least qualitatively, the variation of the scattered signal.

[24] In what follows, we shall mainly be interested in waves approaching the soliton from infinity and exclude trapped groups (which can be important only for waves arising over the soliton). Also we make a natural assumption that the initial distributions of wave action, $N_0(\mathbf{k})$, and energy, $W_0(\mathbf{k})$, decrease with the growth of k, which is almost always true for the range of wavelengths considered, which are shorter than the wind maximum. Consequently, if the wave number of a group increases along its trajectory from infinity (i.e., from some $k = k_0$) to a selected point where it becomes equal to the given $k_f > k_0$, it will bring a larger action and, according to equation (7), larger energy to that point (from a longer-wave part of the initial spectrum) in comparison with its initial (unperturbed) value at the same $\mathbf{k}_f$, $W_0(\mathbf{k}_f)$, and vice versa. This approach reduces the problem to one in which we consider the changes of k along the trajectories as shown in Figures 1–3.

4.2. One-Dimensional Processes

[25] We again begin from a one-dimensional case, $k_y = 0$, and describe the variations of spatial distribution of $W(\xi)$ with the growth of the soliton amplitude. We shall first concentrate on the vicinity of the soliton peak.

[26] First is the case of relatively small η_0 shown in Figure 1a. In this figure, the wave numbers in the range of 570 rad/m to 65 rad/m (wavelengths 1.1 cm to 9.7 cm) at $\xi = 0$ move from infinity to somewhere between the saddle and the center. For these groups, k has a maximum over the soliton; hence, as follows from the above consideration, N and W are larger than they are in the absence of IW. This creates a positive contrast.

[27] For longer waves, with $k < 11$ rad/m, or $\lambda > 58$ cm, and for shorter ones, with $k > 570$ rad/m, or lengths below 1.1 cm, when the trajectories move below or above the equilibrium points, wave number decreases; this means that N and W decrease with respect to their unperturbed values at the same k (negative contrast).

[28] In the range of $11 < k < 65$ rad/m (wavelengths 9.7 cm to 58 cm), the groups are trapped inside the separatrix and move around the center. They are irrelevant to the groups coming from infinity but describe the behavior of waves excited over the soliton.

[29] At the slopes of the soliton, the groups are reflected (blocked) and do not reach the IW peak. It is seen that k grows at the frontal slope and decreases on the rear one. Correspondingly, W increases in comparison with its unperturbed value in the first case and decreases in the second. Note that we do not specially discuss the known

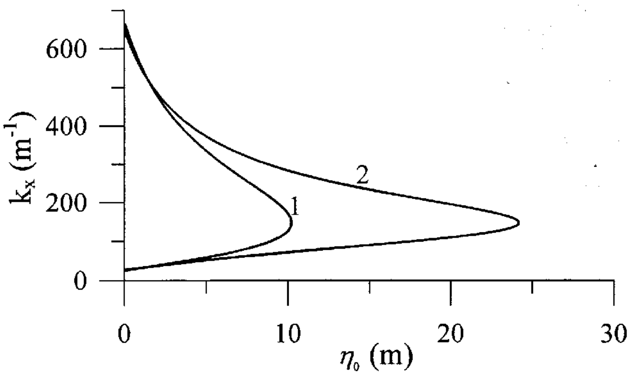

Figure 4. Borders between the areas of increase and decrease of W over the soliton peak ($\xi = 0$) in (k_x, η_0) space for one-dimensional case for $\Delta\rho/\rho = 0.002$, $h_1 = 5$ m, $H = 148$ m. The 1-"nonlinear dispersion" model, (6), 2- KdV approximation.

effect of wave amplitude increase at blocking points (space-time caustics) because it is smeared for waves with a wide continuous spectrum.

[30] Qualitatively, the pattern of trajectories remains the same for larger η_0 (Figure 1b) but the effect is stronger. For all nontrapped waves, there will be a minimum of W over the soliton. Finally, for the case of very strong IW shown in Figure 1c, when the separatrix disappears, W always has a minimum (and a deep one) above the soliton, and reaches a maximum on its front slope. Thus, we have the following pattern of wave behavior in different wavelength ranges (we use the same parameters of a soliton as those in Figures 1a–1c):

[31] For wavelengths of 20 cm to 2.5 m and less than 1.1 cm, for all η_0, $W(\xi)$ always has a minimum over the soliton. For moderate and large η_0 (as in Figures 1b and 1c), these waves have a maximum on the frontal slope of the soliton.

[32] Within these limits, for waves of 1.1 to 20 cm, W increases over the soliton for small η_0. When η_0 becomes larger, the corresponding trajectories coming from infinity do not reach the soliton peak. In this case, W increases over the leading edge and decreases over the trailing edge of the soliton. For large IW amplitudes, when the equilibrium points disappear, the energy minimum is always over the soliton.

[33] Finally, for $\lambda > 2.5$ m, the waves always pass the soliton, always with a slight decrease of W over the soliton. The velocities of these long waves exceed C considerably, and their interaction with the IW current is weak.

[34] As follows from the above consideration, in a practically important range of wavelengths from 1 to 20 cm, the wave energy increases at $\xi = 0$ for weak solitons and decreases for stronger solitons. For the analysis of observational data, it is constructive to define the borderline value of η_0 at which this qualitative change of behavior occurs. As already mentioned, this result depends on whether a minimum or maximum of k exists at the point $\xi = 0$. In other words, the sign of the second derivative $\partial^2 k_x/\partial\xi^2$ at this point determines the effect. From equation (3) it readily follows that the sign of $\partial^2 k_x/\partial\xi^2$ changes when the following equation is satisfied:

$$2C(1-\beta_0)\sqrt{g\left(k_x^2+k_y^2\right)^{3/2}+\nu\left(k_x^2+k_y^2\right)^{5/2}} \\ -gk_x - 3\nu k_x\left(k_x^2+k_y^2\right) = 0, \quad (8)$$

where the values of $\beta_0 = \beta(0)$ and C depend on η_0, according to equations (5) and (6).

[35] The resulting curves corresponding to equation (8) for the soliton model outlined above and, for comparison, for the standard KdV model (in which only the first two terms are left in the right-hand side of equation (6)) are shown in Figure 4. The critical value, η_{0cr}, for which the energy of all waves decreases over the soliton as compared to the nonperturbed state, is achieved at a corresponding critical value of β_0 in equation (8) for which $\partial\beta_0/\partial k = 0$. It is seen that this value is larger for the KdV model than for the strongly nonlinear one: when C decreases, β_{cr} decreases also. (In Figure 1, the saddles and centers move closer to each other for the same soliton amplitude.)

4.3. Oblique Propagation

[36] Now let us briefly discuss the case of an arbitrary angle between the directions of internal and surface wave propagation. In general, the SW spectra are anisotropic, so that the variability of W depends on the direction in a rather

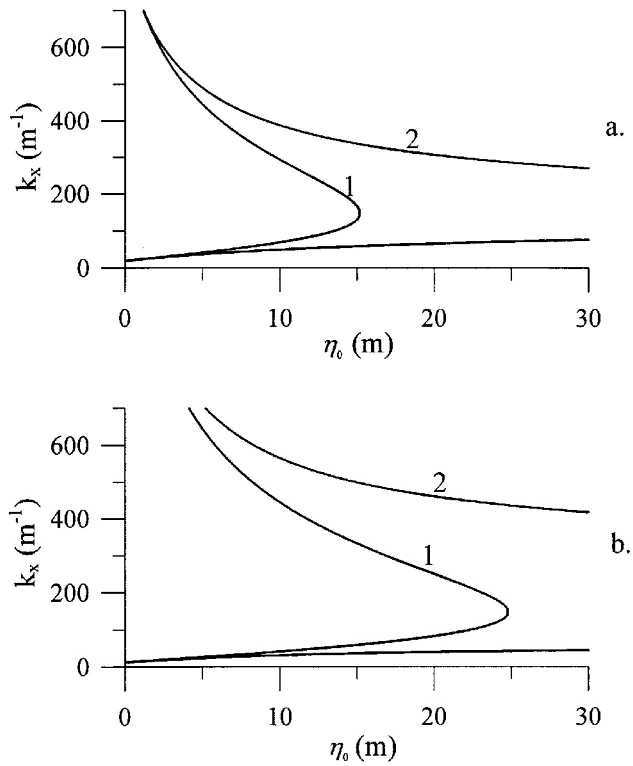

Figure 5. Borders of W increase and decrease areas above internal wave soliton ($\xi = 0$) in (k_x, η_0) space for $\Delta\rho/\rho = 0.002$, $h_1 = 5$ m, $H = 148$ m: (a) $\theta = 30°$ and (b) $\theta = 45°$ (b). The 1-"nonlinear dispersion" model, (6), 2- KdV approximation.

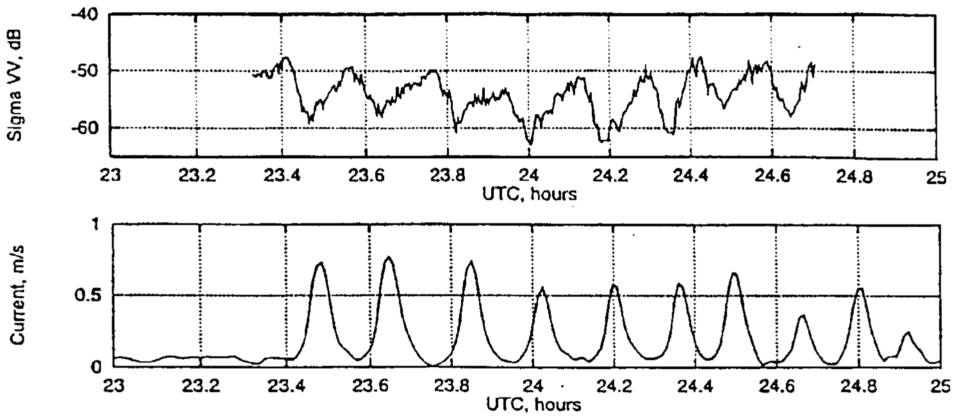

Figure 6. Temporal records of the vertically polarized (VV) signal (top) from the ETL Ka band radar and (bottom) of the subsurface current (below).

complicated way. To obtain a simpler but qualitatively useful result, here we consider an isotropic wave field when the initial spectral density does not depend on θ in the range of wave vectors considered. The dependencies of a "border" amplitude (similar to that in Figure 4) on the wave number for different wave directions, θ, are shown in Figure 5a for $\theta = 30°$ and in Figure 5b for $\theta = 45°$. As in Figures 1–3, the increase of the angle results in the increase of soliton amplitudes that correspond to similar results.

[37] The condition $\partial\beta_0/\partial k = 0$ for an arbitrary angle results in the following:

$$\beta_{cr} = 1 - \cos\theta\left(\frac{(g\nu)^{1/4}\left(6-2\sqrt{3}\right)}{2C\left(4\left(2\sqrt{3}-3\right)\right)^{1/4}}\right). \qquad (9)$$

Here we considered the spectral density transformation for free surface waves. As shown by, e.g., *Hughes* [1978] and *Basovich et al.* [1982], taking into account the wind factor results in the decrease of contrast and an additional displacement of maxima and minima of W with respect to the internal wave profile. This effect strongly depends on the relaxation time for the wind waves and hence, on the wavelength, wind speed, and the wave propagation direction with respect to wind. Such a dependence is complicated [e.g., *Phillips*, 1977; *Hughes*, 1978], but in general this dependence is stronger the shorter the wave considered. For centimeter-range ripples it is typically possible to neglect the wind effect only in special cases such as almost transverse wave propagation to the wind direction (see below). On the other hand, as was experimentally shown in [e.g., *Thompson and Gasparovic*, 1986; *Basovich et al.*, 1988; *Ermakov and Salashin*, 1994], the cascade mechanism can play a significant role when the centimeter and millimeter range SWs are transformed by the internal wave field. Namely, IWs transform decimeter gravity waves (for which the wind relaxation is less significant) which, in turn, modulate "parasitic" capillary ripples arising on the gravity wave crests and propagating toward the wave front. This mechanism is the subject of intense discussions currently. In most cases, the locations of positive and negative contrasts for parasitic ripples roughly coincide with those for a basic gravity wave. In this case, the above results for the behavior of W in decimeter range would describe the geometry of contrasts for centimeter range parasitic waves: amplification over a weak IW soliton and reduction over a strong one. That is, the qualitative pattern of cascade modulation in space is expected to be similar to that for the free waves, although the "boundary" values of IW amplitude, at which the decrease of W above the soliton is changed by its increase, would be different in these two cases.

5. Comparison With Experimental Results

[38] Let us briefly discuss the experimental data. Note that in a majority of experiments in which surface signatures of internal waves were investigated, surface and internal waves propagated in opposite directions. Transformation of SW propagating in the same direction as internal waves was observed by *Hughes and Grant* [1978] and *Shuchman et al.* [1988]. In the former work SWs were modulated by relatively weak IWs generated by a moving ship. The corresponding disposition of minima and maxima of spectral density for the SW agrees with the results of the present work for the case of small β_0. In the latter work, SWs were transformed by intensive IWs. It was found that, in a broad range of wavelengths, the wave energy minimum is situated near the maximum of surface current created by the IW. This is also in agreement with our results.

[39] For the opposite propagation of surface and internal waves, there is no effect of reflection and trapping of surface waves. In this case the formula (13) from *Hughes* [1978] can be used. As follows from that formula, the spectral density of SW must grow on the frontal slope of the internal soliton (with a pycnocline depression) and decrease on its trailing edge. These results are confirmed by the experimental data.

[40] Extremely strong SW modulation by IWs was observed in COPE, as mentioned above. Here we omit a detailed description of that experiment's logistics, which is already given in *Kropfli and Clifford* [1996] and *Kropfli et al.* [1999]. In the context of the present work, it is important that in COPE, a simultaneous measurement of strong internal wave dynamics and of the corresponding backscattered radar signal was carried out. Figure 6 demonstrates

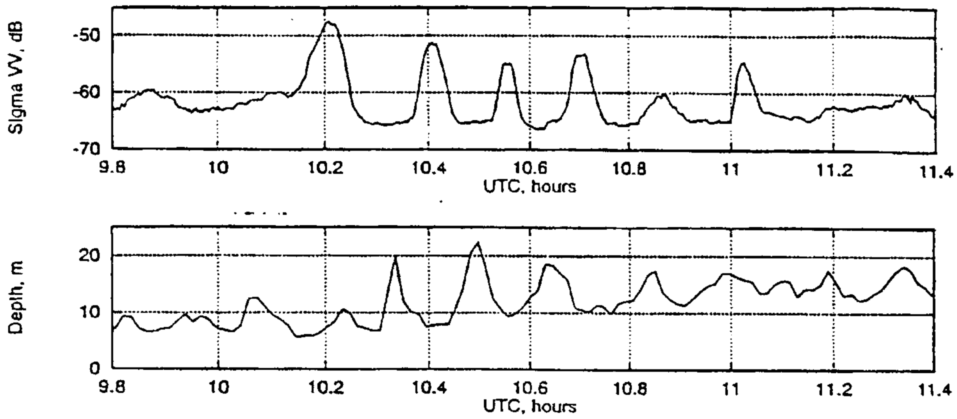

Figure 7. Temporal records of the vertically polarized (VV) signal (top) from the ETL X band radar and (bottom) of the depression of the 15°C isotherm (below).

variability of a backscattered Ka band (8 mm) radar signal with vertical polarization (top figure) due to an internal wave; horizontal current above the pycnocline is shown in the bottom figure in the same timescale. The amplitude of the first three solitons is about 27 m, and of the next four, about 20 m. The radar beam was directed almost perpendicularly to the internal wave front: the angle between observation direction and internal wave propagation direction was approximately 10°. As seen from the figure, minima of the scattered signal correspond to maxima of the current, i.e., to soliton peaks. It is in agreement with the above results regarding variability of 4 mm ripples, for which W decreases over the soliton. (Here the Bragg scattering under small grazing angles is implied as described by *Kropfli et al.* [1999] so that the resonance wavelength is about half of the radar wavelength of 8 mm.)

[41] Figure 7 demonstrates variability of the X band (3 cm) radar signal (top figure) in the field of an internal wave (a displacement of the 15°C isotherm is in the bottom figure). The scattered radar signal *decreases* over the crests of the first three solitons, two of which have amplitudes of about 13 m each and one of about 8 m. At the same time, the scattered signal *increases* over the fourth soliton with an amplitude of about 6 m. From our theory, the increase of W for 1.5 cm ripples above the soliton is replaced by its decrease in roughly this range of internal wave amplitudes.

[42] To obtain quantitative theoretical results regarding the variability of spectral density of SWs, a more straightforward mathematical description is needed. An additional important question is the effect of wind on the modulation of the short waves. For the COPE parameters we solved numerically the well-known kinetic equation for the spectral density of wave action [*Hughes*, 1978]:

$$\frac{\partial N}{\partial t} + \dot{\mathbf{r}}\frac{\partial N}{\partial \mathbf{r}} + \dot{\mathbf{k}}\frac{\partial N}{\partial \mathbf{k}} = \gamma N - \frac{\gamma N^2}{N_0}, \qquad (10)$$

where γ is the growth rate of wind waves, and N_0 is the spectral density of wave action in the absence of internal waves. The last, nonlinear term gives a phenomenological description of nonlinear wave interactions and amplitude-dependent losses (such as those due to wave breaking); it is also necessary for establishment of a stationary wave spectrum. The expressions (1) for variations of $\dot{\mathbf{r}}$ and $\dot{\mathbf{k}}$ were used for calculations along with equation (10).

[43] Some results of calculation of the variability of normalized surface wave spectral density W/W_0 in an asymptotic, quasi-stationary regime are shown in Figures 8 and 9 for SWs with wavelengths of 20 cm and 1.5 cm, respectively. The internal wave was taken in the form of two solitons propagating with a speed of 0.5 m/c. The scale for pycnocline displacement is given to the right of each figure. The wind speed is taken to be 1.5 m/s, the angle between the directions of wind and internal wave propagation is 40°, whereas propagation of surface and internal waves is supposed to be parallel ($\theta = 0$), corresponding to the direction of radar beam. Such a small wind speed was chosen to better demonstrate kinematic effects considered above. The value of W/W_0 is shown in decibels. The Piersson-Moskowitz formula [*Piersson and Moskowitz*, 1964] was used forW_0, and the angular dependence was chosen as $\cos^2(\theta_W/2)$, where θ_W is the angle between the directions of wind and wave propagation.

[44] For Figure 8, the growth coefficient, γ, was calculated according to the Hughes formula [*Hughes*, 1978] obtained as an approximation from several experimental works performed both in laboratory and in situ. It is seen

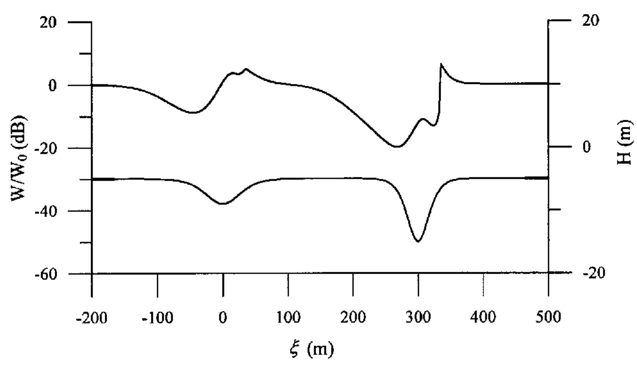

Figure 8. The transformation of spectral density (top) of surface waves with a length of 20 cm in the field (bottom) of internal waves solitons (below). From a numerical simulation.

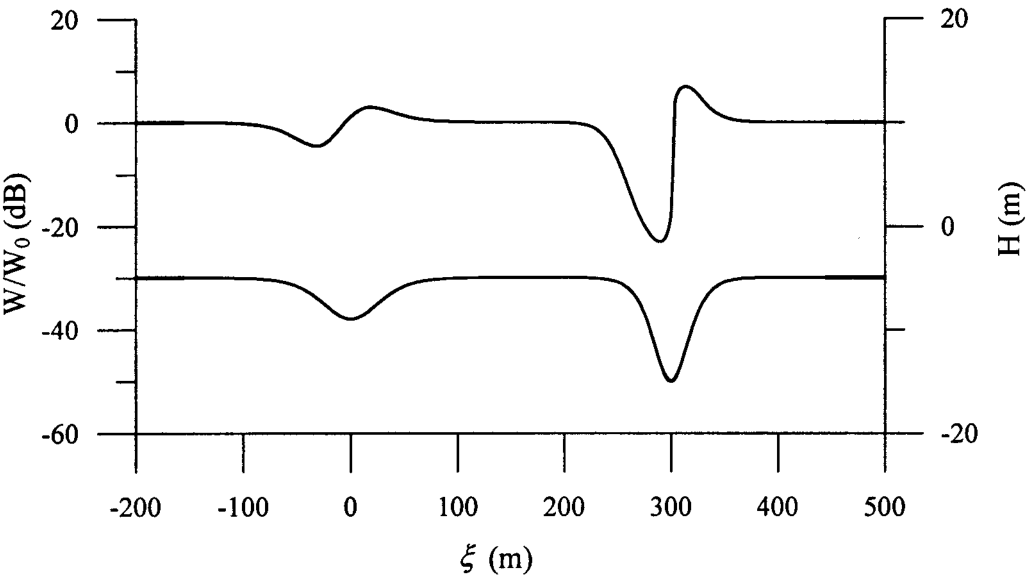

Figure 9. Same as in Figure 8 but for surface waves with a length of 1.5 cm.

from the figure that the minimum of W is situated almost over the peak of the strong internal soliton while it is shifted to the rear side of a weaker soliton: just as it was derived from the qualitative analysis of wave packet trajectories. At the same time, for waves with λ = 1.5 cm, only an insignificant variation of W is obtained from the corresponding calculation. This may testify to the aforementioned cascade mechanism of ripple modulation by internal waves. However, a strong variability of ripples observed in the experiment can be obtained by using another formula; namely, a theoretical expression obtained by Miles [see *Phillips*, 1977] and giving smaller values of γ, which was used for calculations shown in Figure 9. Certainly, choosing different approximations for γ for different spectral ranges of SWs is rather arbitrary but it gives a good agreement with the corresponding experiments, and seems to be justified by the present situation in the wind-wave theory when no well-established expression for γ exists. The variation obtained of W_0/W for 1.5 cm ripples shown in Figure 9 is close to the variability of the X band radar signal observed in COPE.

[45] Note that in both cases, as predicted by the theory, for a strong soliton the minimum of W is situated on the soliton crest and is shifted toward the trailing slope of a smaller soliton.

[46] The values of γ taken above are smaller than those commonly adopted for the SWs propagating along the wind. This is due to the large angle between these directions, and, more specifically, between the directions of the wind and of the radar beam: 40° in the cited COPE measurements. This circumstance strongly decreases the effect of wind on wave modulation. This is confirmed by estimates of different terms in equation (10). These estimates show that even for a small modulation coefficient of SW, each term in the left-hand side of equation (10) can be comparable to the right-hand side responsible for the wind effect. In particular, the order of γ^{-1} for a 1.5 cm long ripple (corresponding to the 3 cm radar Bragg scattering) is about 31 s, whereas a characteristic time of effective wave transformation by IW is about 140 s; it is significantly larger, but the adiabatic effect is still important, as shown by the calculations based on equation (10).

6. Conclusions

[47] The behavior of surface wave groups in the coordinate-wave vector domain varies qualitatively with the increase of internal wave amplitude. For strongly nonlinear internal waves the variation of the surface wave number becomes so significant that, for example, to determine the spectral density variability for initially decimeter-range surface waves, it is necessary to take into account capillary components of the surface wave spectrum. The location of positive and negative contrasts of surface wave energy with respect to the maxima and minima of the isotherm (hence, the isopycnal surfaces) displacement in the IW varies with the increase of internal wave amplitude, so that for strong IW, wave energy has a minimum over the soliton crest or close to it in the entire range of the surface wave spectrum. The theoretical results are confirmed by observational examples. Still, a more detailed overview of observational data is needed for a more substantial validation of the theory and to define the limits of its applicability.

[48] **Acknowledgments.** The authors are grateful to R. Kropfli for valuable discussions at all stages of their work on the paper. The work was partially supported by Russian Foundation for Basic Research (code 99-05-64368). This work was performed while one of the authors (V. Bakhanov) held a National Research Council/NOAA Environmental Technology Laboratory, Boulder, Colorado, Research Associateship.

References

Amick, C., and R. Turner, A global theory of internal waves in two-fluid systems, *Trans. Am. Math. Soc.*, *298*, 431–481, 1986.
Basovich, A. Y., Transformation of the surface wave spectrum due to the action of an internal wave, *Izv. Russ. Acad. Sci. Atmos. Oceanic. Phys., Engl. Transl.*, *15*, 448–452, 1979.

Basovich, A. Y., Adiabatic interaction of surface and internal waves, *Izv. Russ. Acad. Sci. Atmos. Oceanic. Phys., Engl. Transl.*, *18*, 173–175, 1982.

Basovich, A. Y., and V. V. Bakhanov, Surface wave kinematics in the field of an internal wave, *Izv. Russ. Acad. Sci. Atmos. Oceanic. Phys., Engl. Transl.*, *20*, 50–54, 1984.

Basovich, A. Y., and V. I. Talanov, Transformation of short surface waves on inhomogeneous currents, *Izv. Russ. Acad. Sci. Atmos. Oceanic. Phys., Engl. Transl.*, *13*, 514–519, 1977.

Basovich, A. Y., V. V. Bakhanov, and V. I. Talanov, Effect of intense internal waves on wind waves (a kinematic model) (in Russian), in *Effect of Large-Scale Internal Waves on the Sea Surface*, pp. 8–30, IPF AN SSSR, Gor'kiy, Russia, 1982.

Basovich, A. Y., V. V. Bakhanov, D. M. Bravo-Zhivotovskiy, L. B. Gordeev, Y. M. Zhidko, and S. I. Muyakshin, Correlation of changes in the spectral densities of centimeter- and decimeter-length surface waves in an internal wave field, *Dokl. Acad. Sci. USSR, Earth Sci. Ser., Engl. Transl.*, *298*, 216–219, 1988.

Caponi, E. A., D. R. Crawford, H. C. Yuen, and P. G. Saffman, Modulation of radar backscatter from the ocean by a variable surface current, *J. Geophys. Res.*, *93*, 12,249–12,263, 1988.

Choi, W., and R. Camassa, Fully nonlinear internal waves in a two-fluid system, *J. Fluid Mech*, *396*, 1–36, 1999.

Ermakov, S. A., and S. G. Salashin, On strong modulation of capillary-gravitational ripples by internal waves, *Dokl. Acad Sci. USSR, Earth Sci. Ser., Engl. Transl.*, *337*, 108–111, 1994.

Gasparovic, R. F., J. R. Apel, and E. S. Kasischke, An overview of SAR internal wave signature experiment, *J. Geophys. Res.*, *93*, 12,304–12,316, 1988.

Gotwols, B. L., R. E. Sterner II, and D. R. Thompson, Measurement and interpretation of surface roughness changes induced by internal waves during the Joint Canada-U.S. Ocean Wave Investigation Project, *J. Geophys. Res.*, *93*, 12,256–12,281, 1988.

Hogan, G. G., R. D. Chapman, G. Watson, and D. R. Thompson, Observations of ship-generated internal waves in SAR images from Loch Linnhe, Scotland, and comparison with theory and in situ internal wave measurements, *IEEE Trans. Geosci. Remote Sens.*, *34*, 532–542, 1996.

Hughes, B. A., The effect of internal waves on surface wind waves, 2, Theoretical analysis, *J. Geophys. Res.*, *83*, 455–465, 1978.

Hughes, B. A., and T. W. Dawson, Joint Canada-U.S. Ocean Wave Investigation Project: An overview of the Georgia Strait experiment, *J. Geophys. Res.*, *93*, 12,219–12,234, 1988.

Hughes, B. A., and J. F. R. Gower, SAR imagery and surface truth comparisons of internal waves in Georgia Strait, British Columbia, Canada, *J. Geophys. Res.*, *88*, 1809–1824, 1983.

Hughes, B. A., and H. L. Grant, The effect of internal waves on surface wind waves, 1, Experimental measurements, *J. Geophys. Res.*, *83*, 443–454, 1978.

Kropfli, R. A., and S. F. Clifford, The Coastal Ocean Probing Experiment: Further studies of air-sea interactions with remote and in situ sensors, in *IGARSS'96 Proceedings,* pp. 1739–1741, IEEE Press, Piscataway, N. J., 1996.

Kropfli, R. A., L. A. Ostrovsky, T. Stanton, E. A. Skirta, A. N. Keane, and V. Irisov, Relationships between strong internal waves in the coastal zone and their radar and radiometric signatures, *J. Geophys. Res.*, *104*, 3133–3148, 1999.

LeBlond, P. H., and L. A. Mysak, *Waves in the Ocean*, 602 pp., Elsevier Sci., New York, 1978.

Lyzenga, D. R., and J. R. Bennett, Full-spectrum modeling of synthetic aperture radar internal wave signatures, *J. Geophys. Res.*, *93*, 12,345–12,354, 1988.

Ostrovsky, L. A., How to describe strong internal waves in coastal areas, in *Proceedings of the 1998 WHOI/ONR Internal Solitary Wave Workshop*, edited by T. Duda and D. Farmer, pp. 224–228, Woods Hole Oceanogr. Inst., Woods Hole, Mass., 1999.

Ostrovsky, L. A., and Y. A. Stepanyants, Do internal solitons exist in the ocean?, *Rev. Geophys.*, *27*, 293–310, 1989.

Phillips, O. M., *The Dynamics of the Upper Ocean*, 2nd ed., 336 pp., Cambridge Univ. Press, New York, 1977.

Piersson, W. J., and L. Moskowitz, A proposed spectral form for fully developed wind seas based on the similarity theory of S. A. Kitaigorodskii, *J. Geophys. Res.*, *69*, 1581–1590, 1964.

Shuchman, R. A., D. R. Lyzenga, B. M. Lake, B. A. Hughes, R. F. Gasparovic, and E. S. Kasischke, Comparison of Joint Canada-U.S. Ocean Wave Investigation Project synthetic aperture radar date with internal wave observations and modeling results, *J. Geophys. Res.*, *93*, 12,283–12,291, 1988.

Stanton, T. P., and L. A. Ostrovsky, Observations of highly nonlinear internal waves on shelf, *Geophys. Res. Lett.*, *25*, 2695–2698, 1998.

Thompson, D. R., and R. F. Gasparovic, Intensity modulation in SAR images of internal waves, *Nature*, *320*, 345–348, 1986.

Thompson, J. A., and B. J. West, Interaction of small-amplitude surface gravity waves with surface currents, *J. Phys. Oceanogr.*, *5*, 736–749, 1975.

Thompson, D. R., B. L. Gotwols, and R. E. Sterner II, A comparison of measured surface wave spectral modulations with predictions from a wave-current interaction model, *J. Geophys. Res.*, *93*, 12,339–12,343, 1988.

West, B. J., J. A. Thomson, and K. M. Watson, Statistical mechanics of ocean waves, *J. Hydronautics*, *9*, 25–31, 1975.

V. V. Bakhanov, Institute of Applied Physics, Russian Academy of Sciences, 46 Ul'yanov Street, Nizhny Novgorod 603095, Russia.

L. A. Ostrovsky, Zel Technologies/NOAA Environmental Technology Laboratory, 325 Broadway, ETL-0, Boulder, CO 80305, USA. (lev.a. ostrovsky@noaa.gov)